LLAMA: Design and Control of an Omnidirectional Human Mission Scale Quadrupedal Robot

John Nicholson[1], Jay Jasper[2], Ara Kourchians[2], Greg McCutcheon[1], Max Austin[1], Mark Gonzalez[4],
Jason Pusey[3], Sisir Karumanchi[2], Christian Hubicki[1], Jonathan Clark[1]
[1]FSU, [2]JPL, [3]ARL, [4]GD

Abstract— This paper describes the design, control and initial experimental results of the quadruped robot LLAMA. Designed to operate in a human-scale world, this $67kg$-class, all-electric robot is capable of rapid motion over a variety of terrains. Thanks to a unique leg configuration and custom high-torque, low gear-ratio motors, it can move omnidirectionally at speeds over 1 m/s. A hierarchical reactive control scheme allows for robust and efficient motion even under variable payloads. This paper describes the structure of the controller and outlines simulation results that probe the performance envelope of the robot suggesting payload capacities up to one third of its body weight. Initial testing shows robust motion over loose debris and a variety of ground slopes. Videos of the robot may be seen at `https://tinyurl.com/llama-robot`.

I. INTRODUCTION

A. Motivation

Humans are not the fastest or strongest animal, but we are very versatile and adaptable. For millennia, humans have augmented our abilities by utilizing animals to aid us in tasks as diverse as transportation, farming, and hunting. These domesticated animals, such as the dog, horse, donkey, and llama, are not only able to keep up with humans, but working together they extend our capabilities by adding specialized competencies such as superior sensing or providing the strength to carry payloads.

Quadrupedal robots are rapidly approaching these biological exemplars in the both their speed [1], [2], [3] and ability to move through rough terrain [4], [5], [6]. To operate in a human-scale world and carry a meaningful payload, however, these robots need to be fast and of substantial size. BigDog by Boston Dynamics [7], caught the public's attention when it was announced, but limitations, such as its noisy operation and high cost of transport, have precluded widespread adoption.

All-electric legged robots, on the other hand, are quiet and promising. Although many of smaller robots have interesting designs and unique capabilities [8], [9], [10], only a handful of human-scale electric-powered robots have been successfully constructed. These range from early designs, such as Kolt [11], that never made it outside of the lab to more recent commercialized platforms such as Spot and Laikago [12], [13]. Other recent designs of note include ANYmal [4], which has demonstrated autonomous operation in a human environment, and MIT's electric Cheetah I [14], which can run at speeds over 5 m/s [15] and Cheetah III which can blindly climb stairs [16]. While their performance
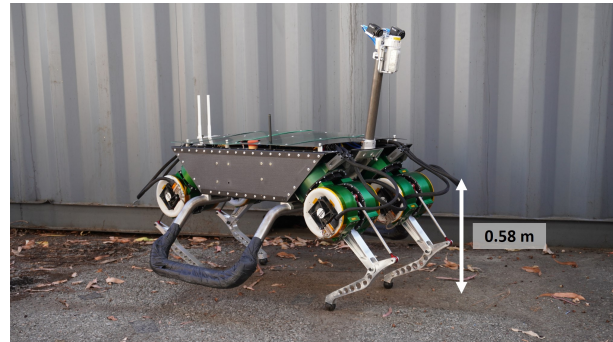

Fig. 1: The all-electric Llama quadrupedal robot weighs $67kg$ total including a $8kg$ $1.2kWh$ custom lithium-ion battery pack. The robot has 12 degrees of freedom with identical large diameter low gear-ratio actuators that each weigh $3kg$.

is impressive, these robots are too small to carry a large payload.

In this paper we introduce LLAMA, a robot designed to be human scale, autonomous, all-electric and capable of carrying a large payload while moving omnidirectionally.

B. Organization

The remainder of the paper is organized as follows: Sec. II describes the robot design including a unique leg orientation which promotes high speed lateral motions and a description of how the leg linkages were optimized to maximize workspace and efficiency. Section III outlines the locomotion controller, a control architecture with software controlled leg compliance and adaptive frequency control that scales well to unknown payloads and efficient motions. In Sec. IV, a simulation of the robot is described and the expected performance limits of the robot and effects of control tuning are explored. Results of the very first robot tests are given in Sec. V, and Sec. VI summarizes the contributions of the paper and directions for future work.

II. ROBOT

A. Overview

The LLAMA quadrupedal robotic platform was created to research the advancement of intelligent autonomous legged locomotion in complex unstructured terrain. LLAMA is a $67kg$ dynamic quadrupedal robot capable of omnidirectional
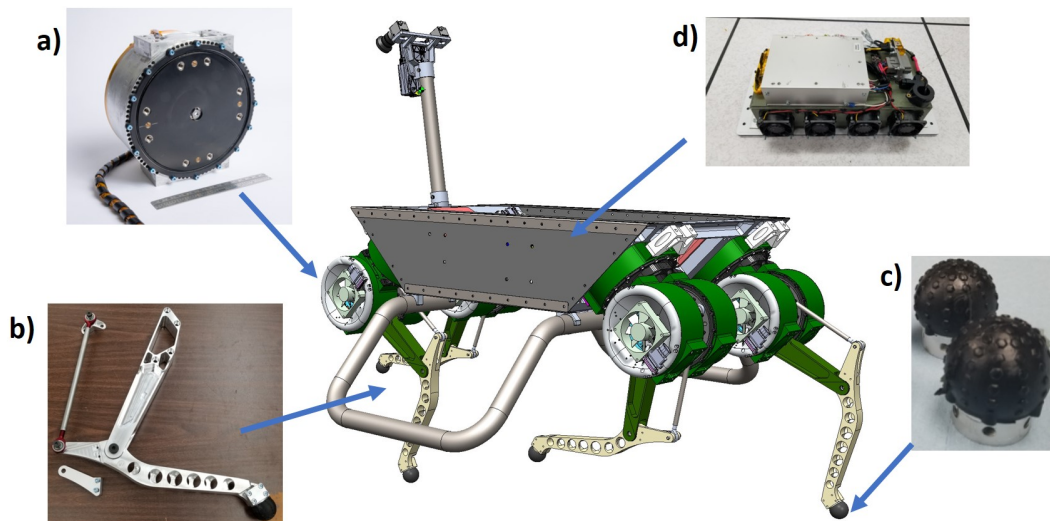
Fig. 2: The all-electric LLAMA quadrupedal robot weighs $67kg$ total including a $8kg$ $1.2kWh$ custom lithium-ion battery pack. The robot has 12 degrees of freedom with identical large diameter low gear-ratio actuators that each weigh $3kg$.

speeds of $1.2m/s$. When standing upright, the robot's shoulders are $0.5m$ high, and its sensor suite is $1m$ above the ground.

Each leg is driven by three identical electric actuators (Section II-B) clustered on the proximal end of the leg to reduce inertial loads. These actuators are very lightly geared (5.25:1) to increase torque density while minimizing reflected inertia and providing a strong signal for current-based proprioceptive controllers.

The robot's energy needs are met by a tether or onboard lithium-ion battery pack. The Energy Management Unit (EMU, Section II-C) is responsible for the monitoring and safe (dis)charging of a large capacitor bank that handles the dynamic electrical loads.

The robot's reactive locomotion controller (Section III) is able to traverse terrain using only actuator feedback and the onboard IMU. Thus, the forward-facing exteroceptive sensor suite is minimal; a stereo camera pair and 1-2 LIDAR sensors. All computations for the controllers are completed by the robot's two onboard computers.

B. Actuators

The leg-actuator system of a dynamic robot must balance torque density, impact absorption, and control bandwidth. On LLAMA, this objective was met by utilizing a lightly geared, large diameter motor, with a rigid kinematic chain between the rotor and foot. Each of the identical custom actuators is built around a brushless motor and contains a planetary gearbox, feedback encoders, and a cooling fan.

As shown in Fig. 2a), the motor (ThinGap, LSI-160) was chosen specifically for its thermal performance; a high K_m of $\sim 0.6Nm/\sqrt{W}$ minimizes waste heat generation, while the slotless stator design minimizes thermal resistance out of the windings. A carefully selected 80mm fan cools the actuator by pulling air through the actuator housing, which contains holes that double as heatsink and mass reduction.

The actuators incorporate several design features to enable proprioception. A single stage planetary gearbox (5.25:1) provides torque amplification and high, bidirectional efficiency to improve the accuracy of motor current as a torque signal. The zero-cogging-torque motor also contributes to the accuracy of a current-derived torque signal.

Also crucial for dynamic proprioceptive control is high bandwidth position and velocity feedback. This is provided by a 32,768 count/revolution optical incremental encoder (Quantum Devices) on the motor rotor. This incremental encoder is initialized for commutation by a set of hall sensors, and zeroed with respect to the robot shape on startup by an absolute encoder (Zettlex) attached directly to the actuator output.

The motor controllers (Elmo) for each actuator are located within the chassis of the robot, and communicate with the onboard computer (both receiving commands and sending telemetry) at 1 kHz over EtherCAT.

C. Energy Management Unit (EMU)

The rigid-limbed, quasi-direct-drive, all-electric architecture places challenging demands upon the electrical system. Loads are not only high power (2.2 kW) but also include sharp peaks of both expended and regenerative energy. The Energy Management Unit (EMU), meets these needs by taking in energy from a battery pack (Fig. 2d) or off-board power supply, buffering it in a large capacitor bank (185V, 18mF), and distributing it throughout the robot. This electrical regenerative system is analogous to the passive mechanical spring in its ability to store and release energy during each gait cycle. To aid efficiency research, the EMU provides telemetry at 100Hz.

D. Legs and Feet

The robot's legs have 3 degrees of actuated freedom, one controlling the leg orientation and the remaining two coordi-
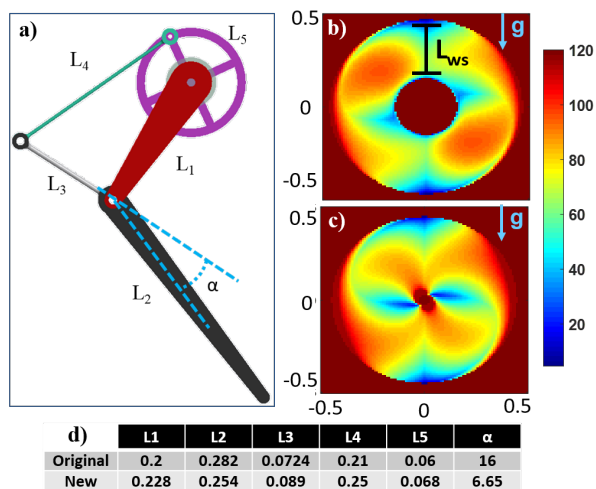
Fig. 3: LLAMA leg kinematic design a) and a gradient of the peak torque required to support an $80kg$ load vertically over the entire workspace for the original leg design for LLAMA b) and the new leg design c). The table d) shows the parameter for the original and new leg values in meters with α in degrees

d)	L1	L2	L3	L4	L5	α
Original	0.2	0.282	0.0724	0.21	0.06	16
New	0.228	0.254	0.089	0.25	0.068	6.65

nating the aluminum, coaxial 5-bar leg (Fig. 2b). The unique $45°$ orientation of the proximal motor is a compromise to enable 3DOF foot motion while minimizing both structural and motor loads. The lower leg design is composed of a "shin" link attached to the rubber foot end-effector (Fig. 2c). The leg's kinematics are governed by six parameters, lengths $L1$ through $L5$ and angle α. Fig. 3a and d tabulates the parameters for the two revisions of the leg geometry that were built and tested.

The optimization of the linkage design follows the process used on BOBCAT [17]. Targets for leg operation were drawn from reduced-order (or *template* [18]) models of LLAMA running. A bipedal SLIP model utilizing walking gaits centered at heights of 18.75, 27.5, and $36.25cm$ and a $3.5Hz$ running gait centered at $27.5cm$ provided the target leg positions, velocities, and forces.

These were mapped to the kinematics of the LLAMA 5-bar and optimized using a particle swarm optimization. The optimization bounded the kinematic parameters of the links $L1$ - $L4$ from 5 to $30cm$. Link $L5$ was bounded from 5 to $6.8cm$ (as it is constrained by the diameter of the actuator) while the angle α was bounded between angles of 0 to $60°$. The cost function used was:

$$Cost = \frac{\tau_{Pk}}{L_{ws}}(|1.5 - \frac{W_1}{W_1 + W_2}|). \tag{1}$$

The combined cost function has 3 factors: minimization of peak torque (τ_{Pk}) required for the gait, maximizing the workspace size (L_{ws}), and distributing the average work between the motors (W_1 and W_2) for the gait. In order to produce legs that did not significantly decrease the workspace size, an additional hard boundary was imposed, disallowing legs with minimum lengths longer than $15cm$ and maximum

lengths shorter than $45cm$. Any leg that violated the motor constraints or did not have a large enough workspace was given a high cost. The optimized kinematic parameters are shown in Fig. 3d.

The comparison between workspace size and peak torque distribution of the original leg and optimum leg design is shown in Fig. 3b and c respectively. The new leg increased the total workspace area by 42% by shortening the minimum leg length from $15.5cm$ to $3.76cm$. The new leg (see Fig. 2b) also reduced the requisite peak torque for the desired behaviors by an average of $10.5Nm$, enabling the $3.5Hz$ running gait (which saturated the actuators on the original design).

The feet (Fig. 2c) were designed with a textured surface made of a thick urethane layer cast around a polycarbonate core at the tip of the leg. The polycarbonate core provided rigidity for stability and the urethane rubber layer allowed high frequency noise attenuation to counter foot impacts during each step and sufficient grip to navigate complex surfaces.

III. HIERARCHICAL REACTIVE CONTROL ARCHITECTURE

LLAMA's locomotion software is a reactive controller with a hierarchical architecture shown in Figure 4. Layers consist of i) a local navigation layer that runs at 2-10Hz (different sub-components at different rates) ii) a control layer that runs at 300Hz consisting of body level velocity control (Capture Point), posture adaptation to slopes (Posture Control) and leg level disturbance rejection (Admittance Control), and iii) actuator motor controllers running 5 kHz PD controllers (Motor Controller).
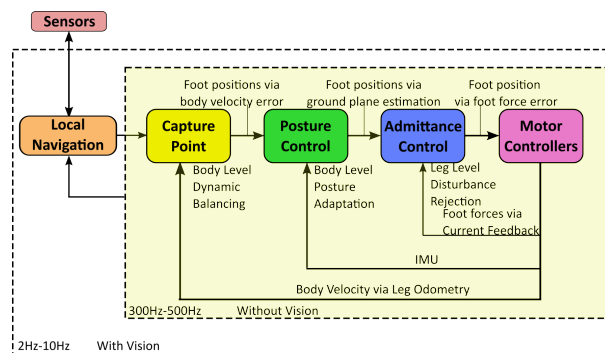

Fig. 4: Baseline control and autonomy architecture

Foot position is the common thread linking the nested loops of the reactive locomotion controller. Each layer adjusts foot position to meet its own goals, and in the end the control scheme treats the plant as a position controlled system. Each joint is controlled at a high bandwidth via a PD loop to compensate for friction and other higher order effects. Actuator-to-actuator manufacturing artifacts are handled via this high-bandwidth PD loop without requiring accurate friction models or system identification as would be needed with current control. Walking gaits are generated via feed-forward pattern generation within the control layer (after

posture control and before admittance). Each of the layers are introduced and discussed in following sub-sections.

The sum of these layers produces $x^R_{f_i cmd}$; where $x^R_{f_i nomPC}$ originates from the posture control layer, ∂x^R_{ff} from the capture point control, and ∂x^R_{fb} from the admittance control.

$$x^R_{f_i cmd} = x^R_{f_i nomPC} + \partial x^R_{ff} + \partial x^R_{fb} \qquad (2)$$
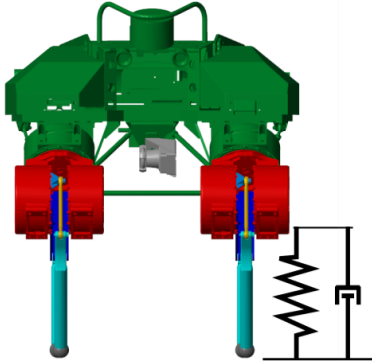
A. Admittance Control

Fig. 5: Admittance Control makes LLAMA's legs react in a spring like manner

The main novelty of the architecture is the middle admittance control layer, which adjusts motor controller position set-points to track a desired force signal. This control loop is effectively a low-bandwidth force feedback loop around a high-bandwidth soft position feedback loop. The desired force is a superposition of static equilibrium and dynamic stability correction terms (proportional controller on body orientation error). The effect is dynamically changing system compliance, crucial in scenarios with uneven and unknown payload distributions on the robot.

Legged robots in rough terrain need to exhibit "soft" behaviors so unexpected interactions with the environment do not cause damage or loss of stability. Simply setting soft motor controller gains is not a viable solution due to loss of control authority. Instead, "medium stiffness" motor controller gains were used while relying on the admittance's variable compliance capabilities to balance robustness and control authority.

Active compliance at the leg level can be achieved via admittance or impedance control frameworks. The former uses force measurements to adjust position set-points and later uses position feedback to adjust force or torque set-points. Both frameworks require forward models for inverse statics or inverse dynamics to either generate leg force set-points or to generate actuator torque commands. The admittance paradigm was chosen for LLAMA as this is less sensitive to accuracy of system modeling which is important to handle unknown payloads. The high bandwidth position feedback at the actuator level also compensates for variations in actuators due to imperfect manufacturing.

At the lowest level, admittance is a force feedback loop which modifies foot position set-points, post gait generation, based on the foot force error signal. As seen below, ΔF^R, is the difference between the expected foot force, F^R_{des}, and the current foot force, F^R_{Cur}, where the superscript R is used to show it is referencing the Robot frame.

$$\Delta F^R = F^R_{des} - F^R_{Cur} \qquad (3)$$

In particular, F^R_{des} is defined as the forces required to support the body with the legs currently in contact with the ground. This term also utilizes the body orientation error to help stabilize the robot. Using the foot force error, the feedback term for determining the commanded foot position ∂x^R_{fb} is defined as

$$\partial x^R_{fb} = K \Delta F^R \qquad (4)$$

where K is a set of control gains defined to reduce contact spikes and reject disturbances before and after contact occurs.
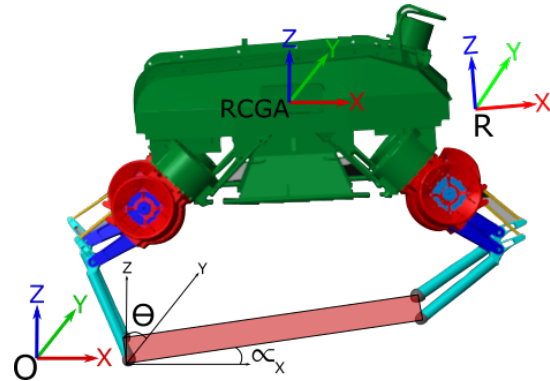
B. Posture Control

Fig. 6: Posture Control adjusts LLAMA's body orientation based on the ground plane estimation. This displays how the Robot Centered Gravity Aligned frame (RCGA) is the translation of the inertial frame (O) to the center of the robot. The robot frame (R) uses the ground plane estimation to determine its rotations from the inertial frame.

LLAMA is expected to traverse constantly changing terrains. Posture control takes as input a ground plane estimate in a gravity aligned inertial frame (Robot Centered Gravity Aligned, RCGA), orients the chassis parallel to this ground plane (increasing workspace), and shifts the center of mass above the center of pressure (increasing stability). Posture control outputs a new nominal foot position $x^{R_{new}}_{i nom}$, which forms an offset to feed-forward gait generation. The ground plane estimate is determined from the positions of feet in contact[1]. The new nominal foot positions are given as follows:

$$x^{R_{new}}_{i nom} = \left(e^{\xi^R dT} \right)^{-1} x^{R_{cur}}_{i nom} \qquad (5)$$

[1]Note that at least three feet are required to be in contact to estimate the ground plane. A small amount dwell/quadruple support phase ensured this requirement.

where $x_{i\,nom}^{R_{cur}}$ is the current foot command. Given $T_{R_{new/old}}^{O}$ which are the transformation matrices representing new and old robot poses and $T_{R_{new}}^{R_{cur}}$ is the correction. $e^{\xi^R dT}$ represents a exponentiated twist form of the correction. See equation below:

$$T_{R_{new}}^{O} = T_{R_{cur}}^{O} T_{R_{new}}^{R_{cur}} = T_{R_{cur}}^{O} e^{\xi^R dT} \tag{6}$$

ξ^R is a correction twist on the body pose to align with the ground plane and shift the body's center of mass. The twist is defined in the current robot frame, R. A description of the different reference frames can be seen in Figure 6.

$$\xi^R = \begin{bmatrix} \nu^R \\ \omega^R \end{bmatrix} = \begin{bmatrix} K_v F_{des} \\ K_\omega M_{des} \end{bmatrix} \tag{7}$$

Here, ν^R and ω^R are the translational and angular velocities, K_v and K_ω are the velocity gains, M_{des} is a virtual body correction moment, and F_{des} is a virtual body correction force. F_{des} is defined using the error between the center of pressure of the robot, and the center of mass projected along gravity. The desired moment, M_{des}, is defined with a proportional controller on the orientation of the current nominal posture ($q_{R_{nom}}^{RCGA}$) with the desired posture given by the ground plane. The moment is generated by transforming the error quaternion ($(q_{nom})^{-1} q_{des}$) to angle axis form.

C. Capture Point Control

The capture point layer adjusts the magnitude and direction of footsteps to control body velocity. This also rejects external disturbances; anything from debris on the ground to the robot getting knocked by an unknown object. The capture point control law is

$$p = p_d + (1 + k_p)(\xi - \xi_d) \tag{8}$$

where p is the virtual foot location at the center of mass, p_d is a feed-forward step based on the desired velocity of the robot, and $(\xi - \xi_d)$ is the velocity feedback term. In addition k_p is a control gain used, which must be positive to stabilize the robot. The Instantaneous Capture Point (ICP) control used here was crafted using a similar method to those in [19].

ICP is used to determine the feed-forward gait generation, ∂x_{ff}, as function of the master clock phase, ϕ, the foot phase offset, $\partial \phi_i$, the half step size, a, step lift, b, and step direction, φ. The half step size, step lift, and step direction are modified by feed-forward reference velocity and feedback capture point control.

$$\partial x_{ff} = f(\phi + \partial \phi_i, a, b, \varphi) \tag{9}$$

IV. SIMULATION

A. Setup

A high fidelity dynamic simulation of the platform was created using a URDF of LLAMA 1.0 and MATLAB's Simscape Multibody framework. LLAMA 1.0's URDF was used in testing while the platform was still in development
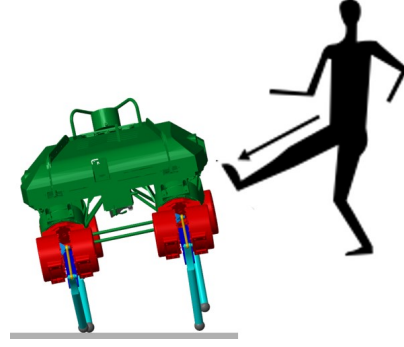

Fig. 7: Capture Point Control allows LLAMA to reject disturbances by correcting for errors in the body velocity of the platform.

and remained to keep consistent results for these studies. The objective of making this model was to determine LLAMA's expected capabilities and to improve control policies for the platform.

Contacts were modeled using the Simscape Multibody Contact Forces Library [20], with the Hunt-Crossley model [21] being used for ground contact, with ground stiffness $K_{ground} = 10^6 N/m$ and ground damping $B_{ground} = 10^3 Ns/m$. A Coulomb friction model is used with static friction $F_{ST} = 1$ and kinetic friction $F_{KE} = 0.7$. These contact models were selected based on previous modeling studies[22]. To constrain the actuator capabilities, a DC motor model was used on each actuator, with actuator torque τ limited by by

$$\tau = T_{Stall} - \omega \frac{T_{Stall}}{W_{NL}}, \tag{10}$$

where ω is the angular velocity, $T_{Stall} = 115Nm$ is the stall torque after gearing, and $W_{NL} = 182.39RPM$ is the no load speed after gearing based of the actuators described in Section II-B. In addition, all simulation runs were constrained by the electrical power limitations of the physical robot. Electrical input power P for each actuator is given by

$$P = \omega\tau + \left(\frac{\tau}{K_t}\right)^2 R_m, \tag{11}$$

and includes both the mechanical power (1st term) and the power loss due to heat (2nd term). The winding resistance is $R_m = 10.8\Omega$ and the torque constant is $K_t = 1.95$. The gear ratio for the motors is $GR = 5.25$.

B. Foot Trajectory

Two foot trajectories were tested in Simscape, the half-moon trajectory and the triangular trajectory, shown in Figure 8. At higher speeds, the triangular gait was found to be more efficient, achieving a minimum cost of transport of 1.55 versus the half-moon trajectory's minimum COT of 1.9. From the foot trajectory path, it can be seen the triangular trajectory produces a footpath that keeps most of the stride moving forward, similar to behavior found in biology [23].
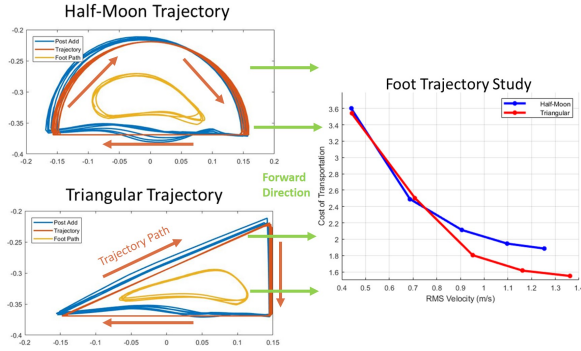
Fig. 8: Testing two different trajectories to use within the Hierarchical controller. While the half-moon trajectory achieves larger steps, the triangular trajectory becomes more efficient at higher speeds

This is different from the half-moon trajectory where while approaching touchdown the foot velocity has a component opposing the desired body velocity. When focusing on obstacle clearance, the half-moon trajectory can achieve a higher apex foot position over a larger distance. This style is advantageous for trying to clear obstacles the platform might face such as stair climbing. The actual trajectory shrinks relative to nominal due to the admittance control and motor controller PD gains. The intent behind these gains are to have LLAMA step softly when impacting the ground. The remainder of Section IV uses the triangular trajectory.

TABLE I: LLAMA Capabilities

LLAMA Capability		
Parameter	Result	Units
Forward Velocity	1.7	m/s
Minimum COT	1.42	N/A
Lateral Velocity	1.0	m/s
Disturbance Rejection	300	N
Settling Time	2.2	s
Payload	25	kg

C. Velocity and COT

1) Gait Frequency: One of the analysis objectives was estimating and maximizing the platform's velocity. To accomplish this, a range of gait frequencies were tested, as seen in Figure 9a. LLAMA was able to achieve speeds of up to 1.7 m/s using a gait frequency of 4 Hz. These higher speed gaits also become more efficient for the platform, with COT values as low as 1.42. It is worth noting that at lower speeds LLAMA is more efficient using lower stride frequencies.

2) Gait Rate Adaptation: As described in Section III, the capture point algorithm controls body velocity by adjusting the stroke length of each leg. With a fixed gait frequency, longer stroke lengths achieve higher speeds. A disadvantage of this approach is that kinematic limits on stroke length limit robot speed. Using the range of stable speeds and frequencies that were found in simulation, as seen in Figure 9b, a function relating the desired velocity of the robot and gait rate was created.
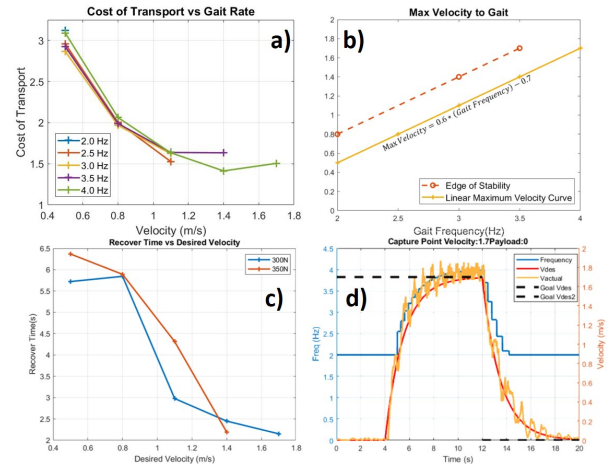

Fig. 9: a) COT vs Gait Rate, we can see higher frequencies result in a small impact to COT at lower speeds, but at higher speeds can achieve stable running. b) Built a speed vs frequency relationship to scale frequency as speed is increased. c) Increasing gait frequency also improves our response to perturbations d) Example showing LLAMA adjusting the gait frequency with increasing speed.

$$Freq = \frac{5}{3}(MaxVel + 0.7), \tag{12}$$

Gradually adjusting frequency at each stride avoids any discontinuities in the foot trajectory. Testing on the real robot confirmed the effectiveness of this control law in enabling higher robot speeds, and it remains enabled.

3) Response to Disturbances: In addition to allowing LLAMA to achieve higher speeds, running at higher frequencies also helps to improve the stability of the robot. With frequency and speed now coupled, Figure 9c shows the settling time from a step disturbance of 300 and 350 N lateral force applied for 0.1 seconds while running at steady state. Running at a higher speed, which results in stepping with a higher frequency, LLAMA is able to return to steady state in 30% of the time it would take running at lower speeds.

D. Additional Performance Metrics

Besides improving the speed and efficiency of LLAMA, the simulation also looked into a variety of other performance metrics. Table I showcases some of those findings. Within the simulation environment LLAMA was also tested running through a series of obstacles, which can be seen in the supplemental video.

V. RESULTS

LLAMA's performance was evaluated in five key areas. These aspects are the robot's Speed, ability to handle Payloads, Efficiency of locomotion, Agility, and Robustness to outside disturbances, or SPEAR. Additionally, LLAMA was tested using various payloads to evaluate the physical platform's maneuverability. Due to constraints with robot usage, the robot capability was not pushed to the same limits achieved within simulation.
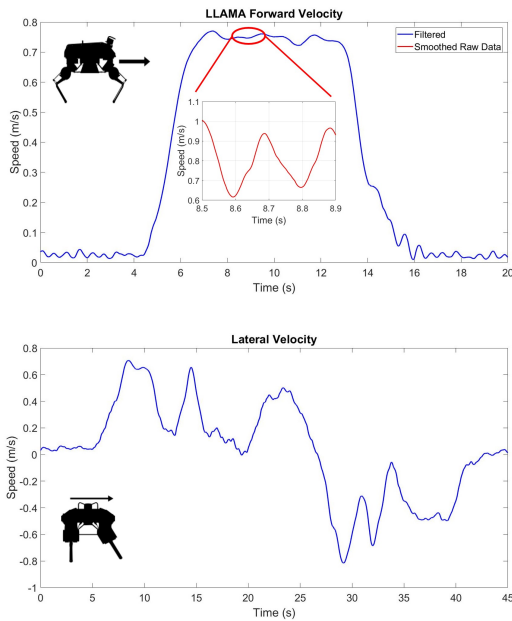
Fig. 10: Velocity of the robot while using adaptive frequency. LLAMA achieves speeds over 1 m/s while also demonstrating SLIP-like running while walking forward and strafing

A. Speed and Agility

Figure 10 shows LLAMA's trotting capabilities. LLAMA maneuvers at an average speed of over 0.75 m/s both in the for-aft locomotion and lateral locomotion. When looking at a single stride, LLAMA is seen performing SLIP like behaviors and reaching speeds of over 1 m/s. LLAMA accelerates from rest to top speed in roughly 2 seconds and decelerates in roughly the same amount of time to prevent damage to the robot. LLAMA can also locomote laterally, reaching peak speeds similar to the platform's forward capabilities.

B. Payload and Efficiency

Figure 11 shows COT and speed for a variety of payloads, demonstrating LLAMA's ability to handle payloads while maintaining efficiency. LLAMA was tested with payloads of 9 kg, and 5.9 kg while traveling at speeds of over 1 m/s. LLAMA is able to carry these payloads without significant changes in cost of transport, maintaining the same level of efficiency as the robot reaches top speeds, for these trials reaching speeds of 1.16 m/s with a mechanical cost of transport of 3.

C. Robustness

Figure 12a shows LLAMA traversing over a series of obstacles. The reactive controller is able to rapidly respond to these unknown disturbances and correct the robot for continued forward locomotion using capture point and admittance control, without any cameras or other external sensors. Figure 12b shows LLAMA traversing off-road sloped terrain. Initial tests show LLAMA can perform omnidirectional walking up slopes of 10-15 degrees without any vision, handling both uphill and downhill inclines.
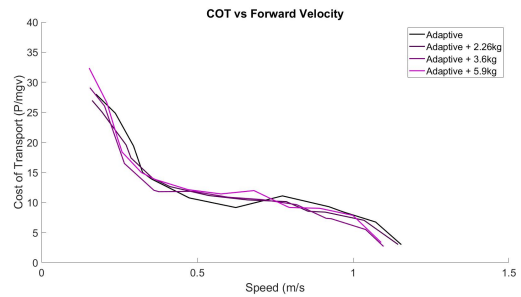

Fig. 11: Cost of transport (P/mgV) performance vs. velocity (m/s) at different payloads ($2.26kg, 3.6kg, 5.9kg$) with adaptive stride frequency
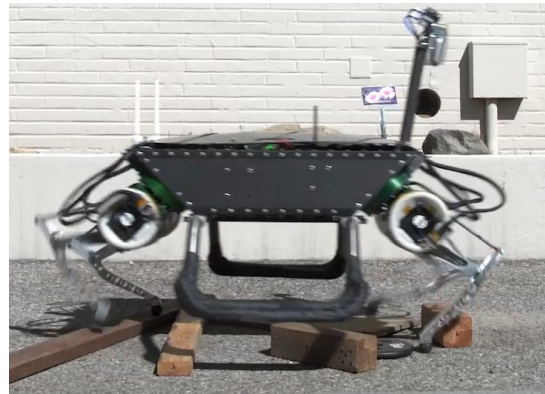

Fig. 12: LLAMA able to (a) walk over various debris without any vision and can recover from disturbances and (b) walk and strafe up and down inclines of up to 15 degrees

VI. CONCLUSION AND FUTURE WORK

This paper presents LLAMA, a human-scale quadruped robot capable of high-speed omnidirectional motion. The all-electric, $67kg$ platform can work in human environments and is equipped with sensing, computational, and payload capabilities suited for autonomous operation. Key aspects of LLAMA's mechanical design include legs oriented at 45 degrees with respect to the ground. This configuration enables reorientation of the leg for high speed lateral motions. The

lower portion of the legs are comprised of a 5-bar design that has been optimized for maximum leg workspace while minimizing the load on the actuators. This combined with custom, large diameter brushless motors allows for large payload capabilities, even with only a small gear reduction. Using a lightly gear motor reduces reflected inertia and enables the use of current-based proprioceptive controllers. Efficiency is improved by a novel energy management unit that allows for transient energy storage and return.

The software for reactive locomotion is a hierarchical control architecture built from three proprioceptive layers. The use of software defined compliance via the admittance layer enables the legs to constantly adapt their stiffness on the fly. The posture control level adjusts body orientation to make the robot robust to ground plane changes, and implementation of a capture-point controller results in dynamic body-level response to perturbation or rough terrain. Together these allow for rapid motion in any direction, and stable maneuvering on slopes and rough terrain–even with minimal exteroceptive sensing. It also results in a loose coupling of performance with system identification. This allows the control architecture to operate even without accurate models of inertial properties, easily adapting to large unknown mass changes due to applied payloads.

Future work includes trials of long range GPS-aided autonomy, investigations into event-driven gait states to improve ground plane estimation, and using exteroceptive sensors to adjust gait timing for conquering terrain that might otherwise challenge a pure-proprioceptive controller. Further hardware tests with the reactive controller may yield the faster locomotion predicted in the simulator, and could be tuned to achieve more aggressive maneuvers such as banked turns or sudden stops. Such improvements would aid the deployability of LLAMA as a human mission capable platform.

ACKNOWLEDGMENTS

REFERENCES

[1] H.-W. Park and S. Kim, "Quadrupedal galloping control for a wide range of speed via vertical impulse scaling," *Bioinspiration & biomimetics*, vol. 10, no. 2, p. 025003, 2015.

[2] J. M. Brown, C. P. Carbiener, J. Nicholson, N. Hemenway, J. L. Pusey, and J. E. Clark, "Fore-aft leg specialization controller for a dynamic quadruped," in *2018 IEEE Int'l Conf. on Robotics and Automation (ICRA)*. IEEE, 2018, pp. 1–9.

[3] A. Spröwitz, A. Tuleu, M. Vespignani, M. Ajallooeian, E. Badri, and A. J. Ijspeert, "Towards dynamic trot gait locomotion: Design, control, and experiments with cheetah-cub, a compliant quadruped robot," *Int'l Journal of Robotics Research*, vol. 32, no. 8, pp. 932–950, 2013.

[4] M. Hutter, C. Gehring, D. Jud, A. Lauber, C. D. Bellicoso, V. Tsounis, J. Hwangbo, K. Bodie, P. Fankhauser, M. Bloesch *et al.*, "Anymal-a highly mobile and dynamic quadrupedal robot," in *Intelligent Robots and Systems (IROS), 2016 IEEE/RSJ Int'l Conf. on*. IEEE, 2016, pp. 38–44.

[5] Y. Fukuoka, H. Kimura, and A. H. Cohen, "Adaptive dynamic walking of a quadruped robot on irregular terrain based on biological concepts," *Int'l Journal of Robotics Research*, vol. 22, no. 3-4, pp. 187–202, 2003.

[6] D. Wooden, M. Malchano, K. Blankespoor, A. Howardy, A. A. Rizzi, and M. Raibert, "Autonomous navigation for bigdog," in *2010 IEEE Int'l Conf. on Robotics and Automation*. IEEE, 2010, pp. 4736–4741.

[7] M. Raibert, K. Blankespoor, G. Nelson, R. Playter *et al.*, "Bigdog, the rough-terrain quadruped robot," in *Proceedings of the 17th World Congress*, vol. 17, no. 1, 2008, pp. 10 822–10 825.

[8] P. Birkmeyer, K. Peterson, and R. S. Fearing, "Dash: A dynamic 16g hexapedal robot," in *Intelligent Robots and Systems, 2009. IROS 2009. IEEE/RSJ Int'l Conf. on*. IEEE, 2009, pp. 2683–2689.

[9] D. W. Haldane, J. K. Yim, and R. S. Fearing, "Repetitive extreme-acceleration (14-g) spatial jumping with salto-1p," in *2017 IEEE/RSJ Int'l Conf. on Intelligent Robots and Systems (IROS)*. IEEE, 2017, pp. 3345–3351.

[10] A. J. Ijspeert, A. Crespi, D. Ryczko, and J.-M. Cabelguen, "From swimming to walking with a salamander robot driven by a spinal cord model," *science*, vol. 315, no. 5817, pp. 1416–1420, 2007.

[11] J. Estremera and K. J. Waldron, "Thrust control, stabilization and energetics of a quadruped running robot," *Int'l Journal of Robotics Research*, vol. 27, no. 10, pp. 1135–1151, 2008.

[12] E. Guizzo, "By leaps and bounds: An exclusive look at how boston dynamics is redefining robot agility," *IEEE Spectrum*, vol. 56, no. 12, pp. 34–39, 2019.

[13] Unitree-laikago. [Online]. Available: http://www.unitree.cc/e/action/ShowInfo.php?classid=6&id=1

[14] S. Seok, A. Wang, M. Y. Chuah, D. Otten, J. Lang, and S. Kim, "Design principles for highly efficient quadrupeds and implementation on the mit cheetah robot," in *Robotics and Automation (ICRA), 2013 IEEE Int'l Conf. on*. IEEE, 2013, pp. 3307–3312.

[15] D. J. Hyun, S. Seok, J. Lee, and S. Kim, "High speed trot-running: Implementation of a hierarchical controller using proprioceptive impedance control on the mit cheetah," *Int'l Journal of Robotics Research*, vol. 33, no. 11, pp. 1417–1445, 2014.

[16] G. Bledt, M. J. Powell, B. Katz, J. Di Carlo, P. M. Wensing, and S. Kim, "Mit cheetah 3: Design and control of a robust, dynamic quadruped robot," in *2018 IEEE/RSJ Int'l Conf. on Intelligent Robots and Systems (IROS)*. IEEE, 2018, pp. 2245–2252.

[17] M. P. Austin, J. M. Brown, C. A. Young, and J. E. Clark, "Leg design to enable dynamic running and climbing on bobcat," in *Intelligent Robots and Systems (IROS), 2018 IEEE/RSJ Int'l Conf. on*. IEEE, 2018.

[18] R. J. Full and D. E. Koditschek, "Templates and anchors: neuromechanical hypotheses of legged locomotion on land," *Journal of experimental biology*, vol. 202, no. 23, pp. 3325–3332, 1999.

[19] M. Krause, J. Englsberger, P.-B. Wieber, and C. Ott, "Stabilization of the capture point dynamics for bipedal walking based on model predictive control," *IFAC Proceedings Volumes*, vol. 45, no. 22, pp. 165 – 171, 2012, 10th IFAC Symposium on Robot Control. [Online]. Available: http://www.sciencedirect.com/science/article/pii/S1474667016336059

[20] S. Miller. (2017) Simscape multibody contact forces library. [Online]. Available: https://www.mathworks.com/matlabcentral/fileexchange/47417-simscape-multibody-contact-forces-library

[21] L. Ding, H. Gao, Z. Deng, J. Song, Y. Liu, G. Liu, and K. Iagnemma, "Foot–terrain interaction mechanics for legged robots: Modeling and experimental validation," *Int'l Journal of Robotics Research*, vol. 32, no. 13, pp. 1585–1606, 2013. [Online]. Available: https://doi.org/10.1177/0278364913498122

[22] M. Y. Harper, J. V. Nicholson, E. G. Collins, J. Pusey, and J. E. Clark, "Energy efficient navigation for running legged robots," in *2019 Int'l Conf. on Robotics and Automation (ICRA)*, May 2019, pp. 6770–6776.

[23] F. L. Moro, A. Spröwitz, A. Tuleu, M. Vespignani, N. G. Tsagarakis, A. J. Ijspeert, and D. G. Caldwell, "Horse-like walking, trotting, and galloping derived from kinematic motion primitives (kmps) and their application to walk/trot transitions in a compliant quadruped robot," *Biological cybernetics*, vol. 107, no. 3, pp. 309–320, 2013.